Trace incorporation of heavy water reveals slow and heterogeneous pathogen growth rates in cystic fibrosis sputum

Sebastian H. Kopf[a,b,1,2], Alex L. Sessions[a,2], Elise S. Cowley[c], Carmen Reyes[d], Lindsey Van Sambeek[c], Yang Hu[c], Victoria J. Orphan[a], Roberta Kato[d], and Dianne K. Newman[a,b,c,2]

[a]Division of Geological and Planetary Sciences, California Institute of Technology, Pasadena, CA 91125; [b]Howard Hughes Medical Institute, California Institute of Technology, Pasadena, CA 91125; [c]Division of Biology and Biological Engineering, California Institute of Technology, Pasadena, CA 91125; and [d]Pediatric Pulmonology, Children's Hospital Los Angeles, Los Angeles, CA 90027

Effective treatment for chronic infections is undermined by a significant gap in understanding of the physiological state of pathogens at the site of infection. Chronic pulmonary infections are responsible for the morbidity and mortality of millions of immunocompromised individuals worldwide, yet drugs that are successful in laboratory culture are far less effective against pathogen populations persisting in vivo. Laboratory models, upon which preclinical development of new drugs is based, can only replicate host conditions when we understand the metabolic state of the pathogens and the degree of heterogeneity within the population. In this study, we measured the anabolic activity of the pathogen *Staphylococcus aureus* directly in the sputum of pediatric patients with cystic fibrosis (CF), by combining the high sensitivity of isotope ratio mass spectrometry with a heavy water labeling approach to capture the full range of in situ growth rates. Our results reveal *S. aureus* generation times with a median of 2.1 d, with extensive growth rate heterogeneity at the single-cell level. These growth rates are far below the detection limit of previous estimates of CF pathogen growth rates, and the rates are slowest in acutely sick patients undergoing pulmonary exacerbations; nevertheless, they are accessible to experimental replication within laboratory models. Treatment regimens that include specific antibiotics (vancomycin, piperacillin/tazobactam, tobramycin) further appear to correlate with slow growth of *S. aureus* on average, but follow-up longitudinal studies must be performed to determine whether this effect holds for individual patients.

slow growth | infectious disease | metabolic heterogeneity | cystic fibrosis | hydrogen isotope labeling

Growth rate is arguably the simplest yet most profound phenotypic parameter that defines microbial existence. It integrates multiple aspects of a cell's physiological state, and is often correlated with how cells respond to challenges presented by diverse stressors, including the immune system and antimicrobial drugs (1–4). Despite recognition that growth rate impacts microbial persistence, very few direct measurements of in vivo generation times exist, in large part because quantifying this parameter within a complex environment presents considerable technical challenges. Chronic infections are often assumed to comprise dormant pathogens, but whether they are truly dormant or merely growing slowly is unknown.

In this study, we focused our attention on the microbial populations within the lungs of patients with cystic fibrosis (CF). CF patients expectorate infected mucus daily, making the in vivo environment directly accessible to experimental investigation. Few prior estimates of microbial growth rates exist for CF sputum (5–7). These estimates are based on detecting the ribosomal RNA (rRNA) content of bacterial cells using fluorescence in situ hybridization (FISH). Kragh et al. (6), for example, showed that the majority of *Pseudomonas aeruginosa* cells in explanted CF lung samples display similar amounts of rRNA to cells in stationary phase, with an rRNA content below that detected for cells in the slowest exponentially growing batch cultures (~0.35 divisions per hour). Although fluorescence intensity can assess growth when the cellular generation time is faster than ~3 h, use of rRNA abundance as a quantitative proxy for slow growth in dynamically changing environments is limited because rRNA content can become completely decoupled from growth (8). This fundamental biological constraint necessitates a new approach to measuring in vivo growth rates.

Utility of Highly Sensitive Stable Isotope Tracers for Application in the Human Host

Stable isotope tracers (e.g., ^{13}C, ^{2}H, and ^{15}N) have been used by geobiologists to study the growth and metabolism of slowly growing microbial populations in poorly accessible and energy-limited habitats at the seafloor (9, 10), and in the deep biosphere (11).

Unlike methods that count cells or particular biomolecules, isotope tracer methods can reveal growth rates that reflect population biosynthetic activity regardless of whether the population is expanding, at steady state, or declining. Isotopic enrichments thus provide a measure of biosynthetic turnover that is independent of total biomass (Fig. 1*A*), making their use well-suited to studies of infected human specimens like CF sputum, where the size of the population can vary due to interactions with other pathogens and the host immune system. Here, we used heavy water ($^{2}H_2O$) because of its advantages as a chemically and nutritionally passive isotope tracer when used at subtoxic concentrations, and measured ^{2}H incorporation into microbial-specific fatty acids by gas chromatography/pyrolysis/isotope ratio

Significance

A major challenge in treating chronic infections is the lack of insight into microbial survival mechanisms in vivo. Many drugs require cells to be doubling rapidly to have their greatest effect, yet the in vivo pathogen growth rate is largely unknown. By labeling freshly expectorated mucus from cystic fibrosis patients with heavy water, we found that the effective growth rates of *Staphylococcus aureus* are at least two orders of magnitude slower, on average, than typically studied in the laboratory, and are extremely heterogeneous at the single-cell level. These findings underscore the need to study slow growth physiology to gain insight into pathogen survival mechanisms, motivated by the hope that such insight will ultimately help improve drug design and clinical outcomes.

Author contributions: S.H.K., A.L.S., and D.K.N. designed research; S.H.K., E.S.C., and Y.H. performed research; S.H.K., A.L.S., E.S.C., C.R., L.V., V.J.O., R.K., and D.K.N. analyzed data; S.H.K. and D.K.N. wrote the paper; and C.R., L.V., and R.K. provided clinical advice and assistance.

The authors declare no conflict of interest.

This article is a PNAS Direct Submission.

[1]Present address: Department of Geosciences, Princeton University, Princeton, NJ 08544.

[2]To whom correspondence may be addressed. Email: dkn@caltech.edu, als@gps.caltech.edu, or sebastian.kopf@colorado.edu.

This article contains supporting information online at www.pnas.org/lookup/suppl/doi:10.1073/pnas.1512057112/-/DCSupplemental.

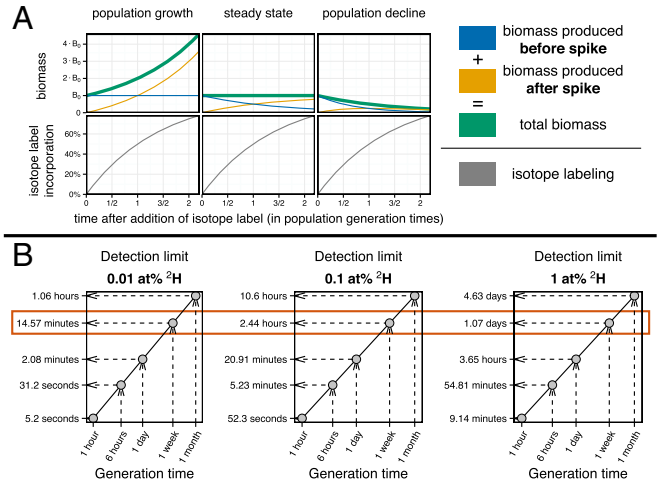

Fig. 1. Using stable isotope tracers to measure microbial activity. (*A*) Model of a microbial population illustrates the change in biomass and the corresponding isotope label incorporation over time after addition of an isotopic spike. In all three scenarios, the isotopic enrichment proceeds identically, allowing determination of the underlying growth rate from isotopic measurements, regardless of total biomass accumulation or decline. (*B*) The minimum incubation times required to detect microbial activity at analytical detection limits of 0.01, 0.1, or 1 atom% ^{2}H above natural abundance for different average generation times of microbial populations exposed to a 10% ^2H_2O labeling solution. See *Supporting Information* for equations.

mass spectrometry (GC/P/IRMS). Other ^{2}H-based measures of microbial activity have been used successfully in laboratory cultures and animal models (12–14) but require high ^{2}H incorporation from heavy water (detection limits 2–3 atom% ^{2}H). GC/P/IRMS, however, can quantify isotopic enrichments well below 0.01 atom% ^{2}H [and under ideal conditions as low as ~0.0001 atom% ^{2}H (15)] enabling much shorter incubation times as illustrated in Fig. 1*B*, making this approach particularly well-suited for application in samples from the human host environment.

Our aim in this study was to develop a method to quantify average and single-cell growth rates for pathogens in chronic infections. For this purpose, we targeted measuring the growth rate of *Staphylococcus aureus* in CF sputum as a proof of principle. Although CF infections are polymicrobial and compositionally diverse, some bacterial species are common (16). *S. aureus* is one of the earliest and most prevalent bacteria detected in infants and children with CF, and has garnered attention in the last decade due to the rise of beta-lactam-resistant strains (methicillin-resistant *S. aureus*, or MRSA) (17). We therefore sought to measure the growth rate of *S. aureus* within freshly expectorated CF sputum both at the population and single-cell level. This approach has the potential to be extended to quantify slow growth rates of diverse organisms in many contexts, ranging from infectious diseases to industrial fermentations to the deep subsurface.

Approach: Methods, Calculations, and Controls

To confidently estimate the in vivo growth rate using an isotope labeling method, a number of factors must be taken into consideration. These include identification of an appropriate biological target molecule, controls to confirm biological compatibility of the isotope label, access of the label to the sample, determination of the extent of label incorporation into the target molecule during biosynthesis, and estimation of how much anabolic activity can be attributed to growth vs. maintenance. Fig. 2 presents an overview of all aspects of our approach and highlights the relevant figures for each step.

Identifying an appropriate biological target for analysis is of primary importance, and several biological considerations must be kept in mind (Fig. 2, marked in green). *S. aureus* synthesizes specific fatty acids (the anteiso methyl branched C_{14} and C_{16} saturated fatty acids, hereafter referred to by their total carbon numbers as *a*-$C_{15:0}$ and *a*-$C_{17:0}$, respectively) that can be distinguished from the human host and most other dominant CF pathogens (Fig. S1), and which are synthesized de novo without recycling (Fig. S2). The lack of fatty acid recycling by *S. aureus* is a critical aspect for our quantitative approach: If organisms build the targeted lipids from exogenous fatty acids, the amount of ^{2}H incorporated from heavy water would be greatly reduced and therefore underestimate population growth rates. By targeting specifically *a*-$C_{15:0}$ and *a*-$C_{17:0}$ for isotopic analysis, we could focus on a suitable marker for *S. aureus*. Because heavy water can be toxic at high concentrations (18), we further tested the susceptibility of *S. aureus* to ^2H_2O to constrain its tolerance and found no adverse effects at doses as high as 35% ^2H_2O (Fig. S3).

For the isotope labeling of clinical samples (Fig. 2, marked in gray), CF sputum collected at Children's Hospital Los Angeles (CHLA) was suspended in a prewarmed PBS isotope labeling solution (with 1% to maximally 30% vol/vol ^2H_2O to stay below the susceptibility of *S. aureus* to ^2H_2O toxicity) within 5–10 min of

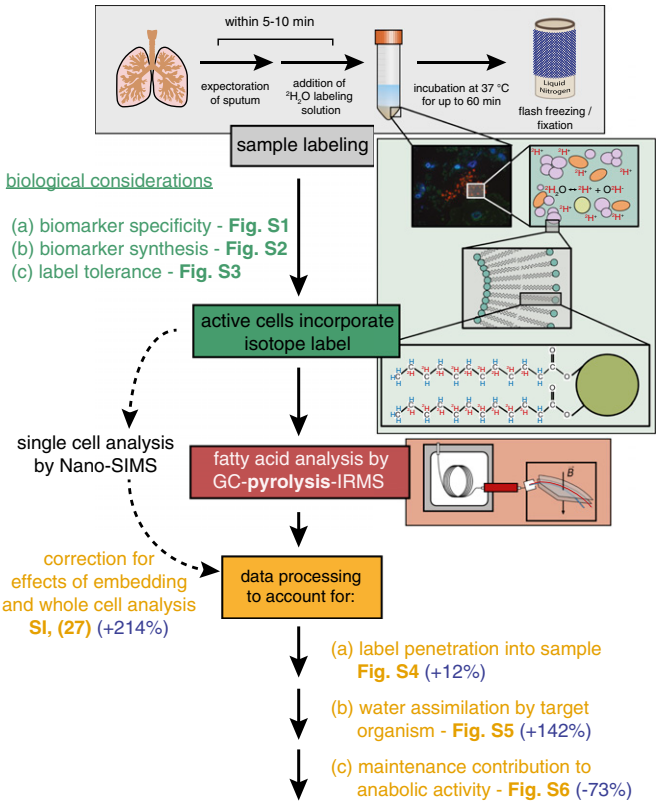

Fig. 2. Schematic illustrating the experimental approach with clinical sample acquisition, biological considerations, and data processing steps. Four stages of the process are highlighted in color: sample labeling at the hospital (gray), incorporation of the isotope label by the cells (green), measurement of specific fatty acids (guava), and quantitative data processing (gold). Specific biological considerations and data reduction steps are listed and point to the relevant figures in the text and *Supporting Information*. In parentheses in blue, we provide what the relative overestimates (+)/underestimates (-) of the growth rates would be for the average clinical sample without the respective corrections. For the uncertainty assessment of all parameters involved in the growth rate calculations, please see Fig. S7. Also noted are the analytical difference and data processing steps required for single-cell measurements.

expectoration, and incubated at 37 °C for up to 60 min for bulk growth rate measurements, and up to 2 h for single-cell analyses. These relatively short incubation times were selected to preserve the in situ sputum environment (19) as closely as possible during the tracer incubation, while still ensuring long enough exposure to the isotope label to allow for measurable incorporation into slow-growing populations.

The resulting isotopic enrichment from growth of *S. aureus* in the presence of the ^{2}H-spiked water was then used to model the apparent growth rate of the pathogen, taking into consideration several potentially confounding factors (Fig. 2, marked in gold). The first concerns the noninstantaneous penetration of the isotope label into a clinical sample. On the time scale of long environmental incubations lasting days or months, the time it takes for heavy water to mix into the sample would be negligible, but, due to the short incubation time (~1 h), this effect becomes relevant, and we parametrized the mixing rate empirically by using isotope label equilibration times in clinical samples (Fig. S4). The second concerns the hydrogen metabolism of *S. aureus* during fatty acid biosynthesis. Although newly synthesized fatty acids follow the isotopic composition of water, this is generally not a 1:1 relationship, because of enzymatic kinetic isotope effects during biosynthesis and because not all H atoms are derived from water during heterotrophic growth. The appropriate value for the resulting water hydrogen assimilation by *S. aureus* growing in clinical samples was determined experimentally in synthetic CF sputum medium (SCFM) (20) following previously established methods (21) (Fig. S5). Finally, because our approach captures the overall anabolic activity, including both the specific growth rate (which signifies true cellular replication) and the maintenance turnover rate (which describes biosynthesis in excess of growth to compensate for degradation and material turnover), quantifying growth requires constraints on the maintenance contribution. We thus grew *S. aureus* in chemostat culture at a controlled, slow growth rate of 0.14 divisions per day (doubling time of 4.9 d) in SCFM, and measured ^{2}H incorporation after a ^2H_2O spike to approximate the contribution of maintenance turnover to fatty acid ^{2}H uptake (Fig. S6).

Using these constraints, we could infer the apparent growth rate of *S. aureus* in clinical samples by numerically fitting the clinical data ($^2F_{fa}$ and ^2F_w, the fractional isotope abundances of ^{2}H measured in fatty acids and sputum water, respectively) to the following equation (full derivation in *Supporting Information*):

$$^2F_{fa}(t) = a_w \cdot \left(^2F_{w_{eq}} - {}^2F_{w_{nat}}\right) \cdot \left[1 - e^{-(\mu+\omega)\cdot t} - \frac{\mu+\omega}{\mu+\omega+k} \cdot \left(1 - e^{-(\mu+\omega+k)\cdot t}\right)\right] + F_{fa_{original}} \cdot \quad [1]$$

This takes into consideration the aforementioned incorporation of hydrogen from water by *S. aureus* (a_ω), rate of label exchange with the mucus (k), and turnover rate (ω). Uncertainties associated with these parameters are discussed in *Supporting Information* (Fig. S7). It is important to note that if the chemical environment within the sputum requires even higher relative rates of fatty acid maintenance/repair than the chemically stable environment of the chemostat, the clinical growth rates would be even lower than currently estimated.

Results and Discussion

Growth Rates of *S. aureus* Populations in Clinical Samples. Having performed these control experiments, we set out to collect a robust cross-sectional dataset from CF patients. Fig. 3 displays the average growth rate of *S. aureus* populations in 37 samples from 16 patients. The growth rate range for each sample is constrained by the *a*-$C_{15:0}$ and *a*-$C_{17:0}$ *S. aureus* specific fatty acid isotope enrichments, and the average rates are calculated from their mass balance. Major potential contributions to these specific fatty acids by other organisms (e.g., *Stenotrophomonas maltophilia*, Fig. S1) were ruled out on the basis of 16S rRNA gene sequencing, which indicated that *Staphylococcaceae* were far more abundant (54% on average, Table S1) than the entire family of *Xanthomonadaceae* to which *Stenotrophomonas* belongs (0.4%). Although the calculated in vivo growth rates of *S. aureus* vary between patients and even between samples from a single patient, all values are 2–100 times lower than the rates at which this organism is typically grown in the laboratory (22). The slow average growth rates suggest that *S. aureus* populations experience environmental constraints within the lung environment. Unlike in many aquatic environments in nature, carbon and nitrogen limitations are less likely to occur within the organic-rich CF sputum environment where millimolar concentrations of free amino acids and other potential nutrient sources have been measured (20). Research into the in situ concentrations and limits of oxygen penetration in sputum points to oxygen availability as a likely dominant growth constraint (19, 23), in addition to inhibition by microbial competitors in the polymicrobial environment (24), as well as effects from continuous antibiotic treatment in these patients and the activity of the immune system (6). Future work in a more expansive longitudinal study of sputum samples artificially amended with different nutrients and antibiotics will help shed light on the factors restricting pathogen growth.

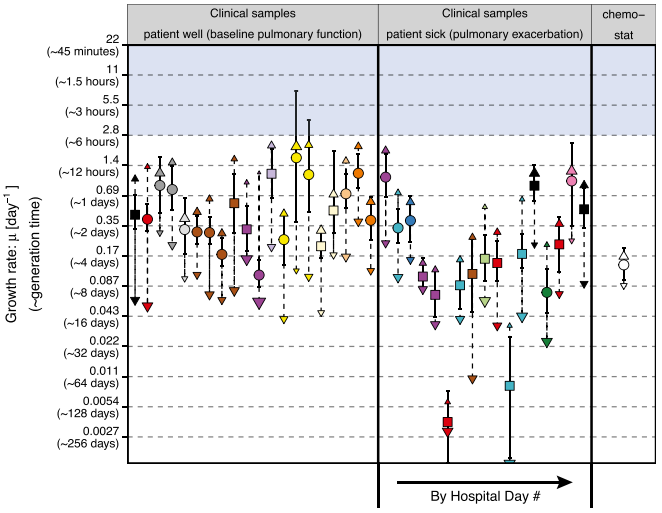

Fig. 3. Average growth rates of *S. aureus* in CF sputum are slow. *S. aureus* population growth rates calculated from the isotopic enrichment of *S. aureus* specific membrane components (*a*-$C_{15:0}$△, *a*-$C_{17:0}$,▽) and the abundance-weighted average isotopic composition for each data point (○/□). Growth rates are plotted on a logarithmic scale. Symbol size illustrates the relative abundance of the component within each sample. Error bars indicate the propagated error estimate on the population growth rate (Fig. S7). Dashed vertical lines connect the *a*-$C_{15:0}$ and *a*-$C_{17:0}$ data points of each sample. Samples are grouped by patient health status (well vs. sick) and color-coded by patient. Samples from sick patients are sorted in ascending order by their hospital stay day. Samples from patients whose treatment regimen at the time included any antibiotics active against *S. aureus* are marked with □ instead of ○. (Antibiotics are vancomycin, oxacillin, piperacillin/tazobactam, amoxicillin/clavulanic acid, trimethoprim/sulfamethoxazole, cefazolin, clindamycin, ciprofloxacin, tetracycline, linezolid, unless *S. aureus* resistance to the antibiotic was reported for the sample; see Table S1 for details.) Separate column (chemostat) shows a representative growth rate from a chemostat culture of *S. aureus* (Fig. S6), demonstrating that it is possible to model slow clinically relevant growth rates in the laboratory. Area highlighted in blue represents the typical range of growth rates studied in laboratory experiments with *S. aureus*.

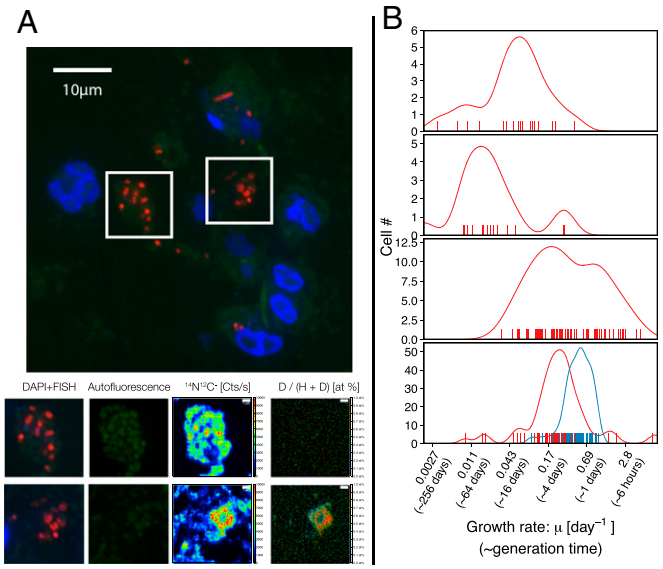

Fig. 4. NanoSIMS analysis reveals that single-cell growth rates are diverse. (*A*) (*Top*) Example of target identification and ^2H enrichment in plastic sections. Frames shown are 10 × 10 μm, (*Bottom*) First column shows microscopy pictures with overlaid DAPI (blue), bacterial EUB338 FISH (red), and sample autofluorescence in the GFP channel (green); second column shows autofluorescence alone (contrast enhanced for mapping to ion image); third column shows the $^{14}N^{12}C^-$ ion image; fourth column shows the fractional abundance image of ^2H. (Scale bar in ion maps, 1 μm.) (*B*) Distribution of single-cell growth rates of *S. aureus* cells (in red) in four clinical samples using the approach described in *Supporting Information*. An unidentified group of bacteria (in blue) was captured in the fourth sample. Bars indicate the measured growth rates of individual cells. Curves illustrate smoothed density distribution function of the data. Growth rates plotted on logarithmic scale.

The data in Fig. 3 also reveal a systematically higher ^2H enrichment of a-$C_{15:0}$ over a-$C_{17:0}$ fatty acids that is more pronounced than the equivalent pattern observed for *S. aureus* grown in chemostat culture in SCFM. Interestingly, *S. aureus* appears to shift its membrane fatty acid composition in response to slower growth (Fig. S8), a phenomenon also observed in other microorganisms (e.g., refs. 25 and 26). This could explain the systematically higher ^2H enrichment of a-$C_{15:0}$ if substantial heterogeneity exists in the underlying staphylococcal population, with slower-growing cells preferentially producing a-$C_{17:0}$ and faster-growing cells producing more a-$C_{15:0}$.

Heterogeneity of Microbial Activity. To test the hypothesis that substantial population heterogeneity exists, we used FISH coupled to secondary ion mass spectrometry (FISH-NanoSIMS) to measure isotope incorporation at the single-cell level (27). Growth rates from single-cell ^2H enrichments were calculated by converting thin-section NanoSIMS measurements to corresponding bulk membrane enrichments (details in *Supporting Information*). Fig. 4*A* shows representative FISH-NanoSIMS images for two cell clusters, illustrating the potential for significantly different in vivo single-cell growth activities on a small scale. The cluster on the left did not incorporate ^2H above background, indicating that the cells were dormant or dead, whereas the cluster on the right incorporated a large amount of ^2H within the 2-h incubation. In this visual field, clusters are microbial (identified by the bacterial FISH probe EUB338), but neither contains *S. aureus* cells.

For the quantitative NanoSIMS analysis shown in Fig. 4*B*, however, we targeted cells that hybridized specifically with an *S. aureus* FISH probe (28). The abundance of *Staphylococcaceae* in the patients whose sputum was analyzed by NanoSIMS ranged from 42 to 56% (Table S1). The smoothed density distribution of the aggregated single-cell growth rates is illustrated for all measured *S. aureus* cells per patient sample. We observed substantial growth rate heterogeneity in all measured samples, with a particularly wide, apparently bimodal distribution observed in the third sample. Sample 4 also contained a large number of unidentified bacteria that were neither *S. aureus* nor *P. aeruginosa*, and appear to be consistently more active than the cooccurring *S. aureus* population (potential candidates from 16S data include members of the *Moraxellaceae* and *Erythrobacteraceae*, with sequence abundances of 13% and 9%, respectively). That *S. aureus* and other bacteria exhibit heterogeneous metabolic activity in vivo is consistent with a growing body of literature documenting the importance of heterogeneity in a wide range of systems (29–31). Moreover, this heterogeneity may help explain why antibiotic treatments are not fully effective: If a reservoir of slowly growing cells exists for any bacterial species being targeted by antibiotics whose efficacy requires fast growth rates, it is not surprising that 25% of pulmonary exacerbations fail to recover to baseline health after treatment with i.v. antibiotics (32).

Correlation with Clinical Parameters. Despite this heterogeneity, we asked whether the average growth rate of *S. aureus* in CF sputum correlates with particular host characteristics and clinical metrics. There were no significant relationships between *S. aureus* growth rates and host age, sex, body mass index (BMI), or lung function (as measured by forced expiratory volume FEV1%) nor with the community abundance of *Staphylococcaceae* or presence of the pathogen *P. aeruginosa* (Table 1). Unexpectedly, *S. aureus* activity showed a statistically significant positive correlation with the day of the patient's hospital stay (i.e., higher apparent growth rates the longer a patient had been in the hospital) with a transient decrease in growth rates early on. Additionally, *S. aureus* populations show significantly higher growth rates in samples from patients who were well (pulmonary function at baseline) compared with samples from patients who were acutely sick (suffering a pulmonary exacerbation; Fig. 3 and Fig. S9).

Intriguingly, on average, *S. aureus* growth rates were significantly lower when patients were taking the antibiotics vancomycin, piperacillin/tazobactam, or tobramycin at the time of sampling compared with when patients were not taking the respective antibiotic (Table 1 and Fig. S10), but no statistically significant trends were observed for the antibiotics aztreonam, colistin, and moxifloxacin. Although tobramycin is primarily used against *P. aeruginosa*, both piperacillin/tazobactam and vancomycin have antistaphylococcal activity. We also note, however, that we were unable to determine whether these correlations held statistical significance for individuals, due to the limited number of patient-specific longitudinal samples (Fig. S10). Generally, at the individual level, being on any antistaphylococcal antibiotics at the time of sampling exhibited no clear trend with respect to growth rate (Fig. 3). Intriguingly, the growth rate of *S. aureus* in some patients at the beginning of their hospital stay appeared to slow, with a return to baseline well before discontinuation of the treatment (e.g., red and teal, Fig. 3). Such dynamics make it tempting to speculate that early during a hospital stay, treatment with anti-Staph antibiotics depresses *S. aureus* growth rates, yet, because patients are simultaneously given many drugs that target various members of microbial community, as other bacteria are eradicated over time, *S. aureus* experiences resource expansion and/or reduced antagonism and begins to grow more quickly. We emphasize, however, that this speculative interpretation requires testing in dedicated longitudinal studies where multivariable regression models can help parse out the interplay between health indicators, treatment regimen, and pathogen growth rate.

Conclusions. Our studies of *S. aureus* in CF sputum reveal that pathogen growth rates can be far slower and more heterogeneous in human infections than previously assumed. Nevertheless, the

range of growth rates that we observe here is largely accessible to experimental replication within laboratory models. Understanding metabolic diversity during slow growth, and how this impacts survival strategies for microorganisms, is a poorly developed but fundamental aspect of microbial physiology and ecology in any environment. What strategies do cells take to control core processes such as transcription, translation, and membrane integrity when persisting in a slow growth mode? How different are these strategies from those that promote cellular homeostasis when nutrients are plentiful and growth is fast? The answers to these and other questions in the context of pathogen behavior in chronic infections are important to understand for practical reasons. For example, *Mycobacterium tuberculosis* is known to persist under hypoxic, nonreplicating conditions (33); encouragingly, inhibition of membrane components that contribute to electron transport and/or proton translocation under these conditions shows promise for shortening the time of tuberculosis therapy (34, 35). Ultimately, a better understanding of how populations grow in vivo is crucial to developing representative in vitro tests of potential therapies for diverse pathogens that infect the human host (36).

Materials and Methods

Study Design. All patients were recruited from CHLA and gave informed consent or assent in accordance with IRB CCI-13000211. Inclusion criteria were a positive diagnosis of CF, ability to expectorate sputum, and recent detection of an infection by *S. aureus* from clinical data.

Sample Collection. Immediately upon expectoration (within 5–10 min), sputum samples were suspended at the hospital in a prewarmed PBS isotope labeling solution (with 1–30% vol/vol ^2H_2O), and incubated at 37 °C for up to 60 min. Microbial growth activity in samples for lipid analysis was arrested by flash-freezing in liquid nitrogen at the end of sample incubation, and samples were preserved at −80 °C. Typically, most pediatric patients could not expectorate more than 0.5–1 g of sputum, but when sufficiently large sputum samples (>0.6 g) were expectorated, the sample was divided before isotope labeling with a scalpel or by transfer with a large syringe. Samples for single-cell analysis were treated the same as bulk samples, except for extension of incubation times up to 2 h (with 10–15% ^2H_2O), and arrest of microbial activity at the end of incubation by transfer to a freshly thawed 1% formaldehyde solution in PBS. Just before sample preservation, the residual labeling solution was collected and filter-sterilized for water isotope analysis.

Isotope Notation. Isotopic measurements were recorded in the conventional δ-notation ($\delta D = \delta^2 H = [(^2R_{sample} - {}^2R_{ref})/{}^2R_{ref}]$) relative to the international reference VSMOW [$^2R_{VSMOW} = {}^2H/{}^1H = 0.00015576(37)$]. To allow consistent reporting and exact mass balance calculations, all measurements were converted to fractional abundances F ($^2F = [^2H/(^1H + {}^2H)]$) using the relation $^xF_{sample} = [^xR_{sample}/(1 + {}^xR_{sample})] = [(\delta^x + 1)/(1/{}^xR_{ref} + \delta^x + 1)]$ and are reported in atom percent (atom%). Data quantification and evaluation of analytical uncertainties are discussed in more detail in *Supporting Information*.

Water Isotope Analysis. The water hydrogen isotopic composition (^2F_w) of all samples was measured using a Los Gatos Research DLT-100 liquid water isotope analyzer. Samples were analyzed in at least three replicate analyses with 10 injections each. Samples close to natural abundance isotopic composition were calibrated against four working standards (δ^2H values: −117‰, −11‰, +290‰, +1,270‰) that in turn were calibrated against the VSMOW, GISP, and SLAP international standards (38). Heavily enriched samples from isotope tracer solutions were beyond the linear response range of the instrument and were analyzed by dilution with water of known isotopic composition.

Fatty Acid Analysis. Frozen sputum samples were lyophilized for at least 48 h. Homogenized dry powder was weighed into ∼40-mg aliquots (or the maximum available amount), and spiked with 10 μg 21:0 phosphatidyl choline as a phospholipid extraction standard. Samples were transesterified in the presence of a base catalyst (0.5M NaOH in anhydrous methanol) at room temperature for 10 min (39). Free fatty acids and aldehydes are not esterified under basic conditions, which prevents the derivatization of fatty acids from degraded materials in the sputum sample, as well as the derivatization of abundant aldehydes, which interfere chromatographically with target analytes. Derivatized fatty acid methyl esters (FAMEs) were extracted into hexane, and concentrated under a stream of N_2 at room temperature. Because primary target analytes (*a*-$C_{15:0}$ FA and *a*-$C_{17:0}$ FA) typically constituted less than 1% of host-derived fatty acids, the high abundance of host material [primarily $C_{18:1}$ FA, $C_{18:2}$ FA, and longer chain (poly)-unsaturated fatty acids] interfered with compound-specific isotope ratio analysis of these compounds due to column overload. The low total amount of target analytes available from most sample sizes precluded the use of elaborate purification steps with low yields or risk of contamination. To remove several major host compounds and increase relative abundance of the analytes sufficiently for isotope ratio analysis, saturated

Table 1. *S. aureus* growth rates vs. health and treatment indicators

Clinical parameter	Samples	Data range	Statistic†	*P* value	Significance
Age	37	9–20 y of age	Spearman (−0.23)	0.2	—
Sex	37	female (8), male (29)	MWW (female > male)	0.3	—
Race	37	Hispanic (21), Non-Hispanic White (11), African-American (5)	Spearman (−0.23)	0.2	—
BMI	33	14.1–21.3 kg/m^2	Spearman (0.18)	0.3	—
FEV1%	37	20–118% predicted	Spearman (0.06)	0.7	—
Pulmonary exacerbation	37	no (20), yes (17)	MWW (no > yes)	0.004	**
Hospital day	15	day 1–30	Spearman (0.53)	0.04	*
P. aeruginosa present‡	32	no (21), yes (11)	MWW (no > yes)	0.1	—
Staphylococcacea‡	32	40–71%	Spearman (−0.12)	0.5	—
Vancomycin§	37	treatment at the time included this antibiotic: no (32), yes (5)	MWW (no > yes)	0.002	**
Piperacillin/tazobactam§	37	treatment at the time included this antibiotic: no (30), yes (7)	MWW (no > yes)	0.003	**
Tobramycin§	36	treatment at the time included this antibiotic: no (11), yes (25)	MWW (no > yes)	0.05	*
Inhaled aztreonam§	36	treatment at the time included this antibiotic: no (27), yes (9)	MWW (no > yes)	0.1	—
Colistin§	36	treatment at the time included this antibiotic: no (27), yes (9)	MWW (no > yes)	0.1	—
Moxifloxacin§	36	treatment at the time included this antibiotic: no (31), yes (5)	MWW (no > yes)	0.3	—

Summary of statistical relationships between *S. aureus* average population growth rate and different health and treatment indicators by Mann–Whitney–Wilcoxon (MWW) test (for binary parameters) or Spearman rank analysis. Spearman's $P < 0$ indicates positive correlation (i.e., faster growth rate with increase of the clinical parameter), and $P < 0$ indicates a negative correlation. See Table S1 for all data, and see Figs. S7 and S8 for correlation plots. Only antibiotics with at least five samples in each category (yes/no) were analyzed. —$P > 0.05$, *$P \leq 0.05$, **$P \leq 0.01$.

†Evaluated by MWW test for binary parameters (sex, pulmonary exacerbation, and *P. aeruginosa* presence; each was evaluated for both alternative hypotheses; the most statistically significant alternative is given) and by Spearman rank analysis for all other parameters.

‡The presence of *P. aeruginosa* was tested in routine clinical selective plating screens. The abundance of *Staphylococcaceae* was assessed by 16S rRNA gene sequencing.

§Vancomycin is used against Gram-positive pathogens including MRSA; piperacillin/tazobactam is used against *P. aeruginosa* and some *S. aureus* (not effective against MRSA); tobramycin, aztreonam, and colistin are mostly used against *P. aeruginosa*; moxifloxacin is a broad-spectrum antibiotic mostly used against mycobacteria.

FAMEs were separated from unsaturated FAMEs using Discovery Ag-Ion solid-phase extraction columns in combusted glass cartridges (Supelco; custom preparation to avoid contaminants from plastic columns). Extracted samples were dried to 1 mL and applied to preconditioned columns, followed by elution of saturated FAMEs in 0.125% acetone in hexane, and monosaturated and disaturated FAMEs in acetone. Separation of unsaturated and saturated fatty acids was quantitative using this procedure. Fractions were evaporated to dryness and resuspended in hexane before analysis.

FAMEs were analyzed by gas chromatography/mass spectrometry (GC/MS) on a Thermo-Scientific Trace DSQ equipped with a ZB-5ms column (30 m × 0.25 mm i.d., film thickness 0.25 μm) and PTV injector operated in splitless mode, using He as a carrier gas at 0.8 mL/min. The GC oven was held at 80 °C for 1 min, ramped at 20 °C/min to 130 °C, and ramped at 5 °C/min to a final temperature of 320 °C (held for 20 min). Peaks were identified by comparison of mass spectra and retention times to authentic standards and library data. Fatty acids are referred to using the nomenclature *z*-$C_{x:y}$, where x is the total number of carbons in the fatty acid skeleton (regardless of structure), y is the number of double bonds, and *z*- is a prefix describing additional structural features of the compound. The position and stereochemistry of the double bonds or cyclopropyl rings was not determined. The isotopic composition of the primary target analytes was measured in the saturated FAME fraction by GC/pyrolysis/isotope-ratio mass spectrometry on a Thermo-Scientific Delta$^+$XP with methane of known isotopic composition as the calibration standard. A multicompound FAME standard was run every four to six samples to verify instrument accuracy and precision. Chromatographic conditions were identical to those from GC/MS analysis except for a thick-film column (ZB-5ms, 30 m × 0.25 mm i.d., film thickness 1.00 μm) and slight modifications to the temperature program to optimize chromatographic separation of *i*-$C_{15:0}$ and *a*-$C_{15:0}$/*i*-$C_{17:0}$ and *a*-$C_{17:0}$ despite peak broadening from isotope labeling and heavy column loading. Samples were injected in highly concentrated aliquots to obtain maximum signal for target analytes. Peaks were identified based on retention order and relative height based on the GC/MS analysis. High-abundance components in the saturate fraction ($C_{16:0}$, $C_{18:0}$, $C_{20:0}$) that were too concentrated relative to target analytes were prevented from entering the source by appropriately timed backflush of the column effluent. Relative proportions of fatty acids for isotope mass balance calculations were determined from peak areas corrected for derivatization and isotopic composition.

Single-Cell Analysis. Immediately upon receipt of samples from the hospital, formaldehyde-fixed sputum samples were transferred to excess PBS solution (10 mL) in a column above an 8-μm sterile filer. The sample was washed by slowly rinsing it with a total of 50 mL PBS solution that was added to the column in 10-mL aliquots and drained by gravimetric or slight vacuum flow through the filter. Samples were suspended in drops of molten noble agar [2% (wt/vol) Difco Agar Noble in 50 mM Hepes buffered filter-sterilized water], solidified by cooling at room temperature, and cut into ∼2-mm^3 cubes. Fixed and washed agar cubes were incubated for at least 1 h at 30 °C in freshly prepared 1mg/mL lysozyme and 50 μg/mL lysostaphin (L2898; Sigma-Aldrich) in 10 mM Tris buffered water to digest *S. aureus* cell wall, washed once in PBS, resuspended in 50% (vol/vol) ethanol in PBS, and dehydrated in 100% ethanol over the course of three exchanges, with final resuspension in 100% for at least 1 h. Ethanol was then replaced twice with 100% Technovit 8100 infiltration solution (64709012; Heraeus Kulzer GmbH) to infiltrate the agar cubes overnight. Agar cubes were finally suspended in airtight 0.6-mL microcentrifuge tubes in Technovit 8100 infiltration solution amended with hardener II reagent and stored at 4 °C for overnight polymerization. Thin sections (1 μm thick) were cut using a rotary microtome. Each section was stretched on the surface of a water drop on polylysine-coated microscope slides and air-dried at room temperature.

FISH was conducted on the plastic thin sections using the universal bacterial probe EUB338 [5′ to 3′: GCT GCC TCC CGT AGG AGT (40)], which hybridizes to bacterial 16S rRNA, probe Sau [5′ to 3′: GAA GCA AGC TTC TCG TCC G (28)], which hybridizes to *S. aureus* 16S rRNA, and probe Psae [5′ to 3′: TCT CGG CCT TGA AAC CCC (41)], which hybridizes to *P. aeruginosa* 23S rRNA. Both probes were specifically designed and tested for use in microbial identification in CF sputum (41, 42). Additionally, probe Non338 [5′ to 3′: ACT CCT ACG GGA GGC AGC (43)], an oligonucleotide complementary to the probe EUB338, served as a negative control for nonspecific binding. Probes EUB338 and Non338 were labeled with the cyanine dye Cy3, probe Sau was labeled with the cyanine dye Cy5, and probe Psae were labeled with fluorescein. All probes were labeled on both the 5′ and 3′ end to increase fluorescence intensity (44). For hybridization, each section was covered with 20 μl of hybridization buffer [0.9 M NaCl, 20mM Tris·HCl at pH 8, 0.01% SDS, 20% (vol/vol) formamide (28, 42)] containing 50 ng of unlabeled oligonucleotide probe BET42a [5′ to 3′: GCC TTC CCA CTT CGT TT (45)] and preincubated for 10 min at 46 °C to reduce nonspecific binding of labeled oligonucleotide probes (41). Probes EUB338 (or Non338), Sau, and Psae were added (5 ng/μL), and samples were incubated in a moisture chamber at 46 °C for 3 h. Stringent washing was performed by incubating the samples in washing buffer at decreased NaCl concentration [225 mM NaCl with 5 mM EDTA, 20 mM Tris·HCl at pH 8, 0.01% SDS (46)] at 48 °C for 12 min. Finally, samples were dipped into ice-cold deionized water to rinse off the salt, air-dried, and mounted in the glycerol-based soft mount Vectashield (Vector Laboratories) (47) with 1.5 μg/mL 4′,6-diamidino-2-phenylindole (DAPI) as a DNA counterstain. Samples were routinely imaged using a Zeiss Axio Imager microscope, and mapped extensively for sample identification and target localization for FISH–NanoSIMS using a Keyence BZ-9000 microscope equipped with a mercury lamp and filter cubes for DAPI, GFP, Cy3, and Cy5. For secondary ion mass spectrometry, samples were made conductive by sputter-coating with a 50-nm layer of gold.

All samples were analyzed with a CAMECA NanoSIMS 50L (CAMECA) housed in the Division of Geological and Planetary Sciences at California Institute of Technology. Cells in plastic thin sections were analyzed using a 1.9- to 3.6-pA primary Cs^+ beam, and were presputtered with a ∼ 200-pA primary Cs^+ beam current (I_{pre}) for 3–15 min (t), depending on the size of the presputtering area (A), to a cumulative charge density of ∼ 30 pC/μm^2 ($I_{pre} \cdot t/A$). Seven masses were collected in parallel ($^1H^-$, $^2H^-$, $^{12}C^-$, $^{13}C^-$, $^{14}N^{12}C^-$, $^{15}N^{12}C^-$, and $^{28}Si^-$) using the configuration reported in ref. 27. Target locations in individual samples were located using the NanoSIMS CCD camera, secondary electron image, and $^{14}N^{12}C^-$ ion maps. For all analyses, the beam was rastered over a square region ranging from 5 × 5 μm^2 to 50 × 50 μm^2 for 5–30 min per analytical plane/frame, and images were collected in 256 × 256 pixel resolution up to 12 × 12 μm^2 and 512 × 512 pixel resolution for larger areas. Presputtering was carried out on a region larger than the analytical frame by at least 2 μm on each side. Analytical parameters including primary beam focus, secondary beam centering, and mass resolution for all ions were verified every ∼30 min. To correct for instrument mass fractionation and matrix effects of the plastic polymer, we calibrated plastic-embedded single-cell measurements against bacterial isotope standards that were analyzed at the same time and were previously presented in detail (27). Data evaluation is discussed in more detail in *Supporting Information*.

The 16S Ribosomal RNA Gene Sequencing. DNA was prepared from ∼1 mg lyophilized sputum samples treated with 2% vol/vol PBS/β-mercapto-ethanol for 2 h at room temperature and Sputolysin (Calbiochem) for 30 min at 37 °C, followed by lysis in 180 μL of buffer ATL (Qiagen Blood and Tissue DNeasy kit) amended with lysostaphin (final concentration 0.14 mg/mL) and lysozyme (final concentration of 2.9 mg/mL) (48) for 2 h at 37 °C, bead-beating with 0.1-mm glass beads for 10 min, and extraction using the Qiagen Animal Tissues Spin Column Protocol with 20 μL proteinase K during overnight incubation. High throughput sequencing was performed as previously described (49). Briefly, purified DNA was amplified in triplicate using 16S rRNA Illumina barcoded primers specific to the V4 region of the 16S rRNA gene. Samples were pooled, and paired-end sequencing was performed on an Illumina MiSeq platform at CHLA. Sequences were demultiplexed and trimmed, and paired-end reads were joined, trimmed according to quality score, and checked for chimeras. Sequences were assigned to de novo OTUs (operational taxonomic units) using uclust (50) to search sequences against the Greengenes database (2014 version), and were assigned if the sequence matched the database at 97% similarity or greater. If a read did not match a database sequence, it was considered unassigned. Taxonomy was assigned at the family level based on the Greengenes matching sequence. The genera *Geobacillus*, *Rhodothermus*, and *Rhodocyclaceae* were considered to be contaminants and were filtered out from the results. Table S1 includes the sequence abundances of the *S. aureus* family *Staphylococcaceae*, and the *S. maltophilia* family *Xanthomonadaceae* (the main organism with partly overlapping fatty acid profiles).

ACKNOWLEDGMENTS. We are grateful to Shawn McGlynn, Ryan Hunter, Abigail Green-Saxena, Yunbin Guan, Alejandro LaRiviere, Ian Booth, Nathan Dalleska, Fadi Asfour, Douglas Li, Kyle McCallin, Sally Ward, Thomas Keens, and patients of the Pulmonary CF Clinic at CHLA for supporting this study. We thank the editor and reviewers for constructive criticism that improved the manuscript. This research was supported by grants from the NIH (Grant 5R01HL117328-03) and the Howard Hughes Medical Institute (HHMI) (to D.K.N.). S.H.K. was an HHMI International Research Scholar, and D.K.N. is an HHMI Investigator.

1. Gilbert P, Collier PJ, Brown MR (1990) Influence of growth rate on susceptibility to antimicrobial agents: Biofilms, cell cycle, dormancy, and stringent response. *Antimicrob Agents Chemother* 34(10):1865–1868.
2. Brown MR, Collier PJ, Gilbert P (1990) Influence of growth rate on susceptibility to antimicrobial agents: Modification of the cell envelope and batch and continuous culture studies. *Antimicrob Agents Chemother* 34(9):1623–1628.
3. Baek SH, Li AH, Sassetti CM (2011) Metabolic regulation of mycobacterial growth and antibiotic sensitivity. *PLoS Biol* 9(5):e1001065.
4. Nguyen D, et al. (2011) Active starvation responses mediate antibiotic tolerance in biofilms and nutrient-limited bacteria. *Science* 334(6058):982–986.
5. Yang L, et al. (2008) *In situ* growth rates and biofilm development of *Pseudomonas aeruginosa* populations in chronic lung infections. *J Bacteriol* 190(8):2767–2776.
6. Kragh KN, et al. (2014) Polymorphonuclear leukocytes restrict growth of *Pseudomonas aeruginosa* in the lungs of cystic fibrosis patients. *Infect Immun* 82(11):4477–4486.
7. Kolpen M, et al. (2015) Denitrification by cystic fibrosis pathogens —*Stenotrophomonas maltophilia* is dormant in sputum. *Int J Med Microbiol* 305(1):1–10.
8. Blazewicz SJ, Barnard RL, Daly RA, Firestone MK (2013) Evaluating rRNA as an indicator of microbial activity in environmental communities: Limitations and uses. *ISME J* 7(11):2061–2068.
9. Wegener G, et al. (2012) Assessing sub-seafloor microbial activity by combined stable isotope probing with deuterated water and ^{13}C-bicarbonate. *Environ Microbiol* 14(6):1517–1527.
10. Kellermann MY, et al. (2012) Autotrophy as a predominant mode of carbon fixation in anaerobic methane-oxidizing microbial communities. *Proc Natl Acad Sci USA* 109(47):19321–19326.
11. Morono Y, et al. (2011) Carbon and nitrogen assimilation in deep subseafloor microbial cells. *Proc Natl Acad Sci USA* 108(45):18295–18300.
12. Berry D, et al. (2015) Tracking heavy water (D_2O) incorporation for identifying and sorting active microbial cells. *Proc Natl Acad Sci USA* 112(2):E194–E203.
13. Kloehn J, Saunders EC, O'Callaghan S, Dagley MJ, McConville MJ (2015) Characterization of metabolically quiescent *Leishmania* parasites in murine lesions using heavy water labeling. *PLoS Pathog* 11(2):e1004683.
14. Fischer CR, Bowen BP, Pan C, Northen TR, Banfield JF (2013) Stable-isotope probing reveals that hydrogen isotope fractionation in proteins and lipids in a microbial community are different and species-specific. *ACS Chem Biol* 8(8):1755–1763.
15. Sessions AL (2006) Isotope-ratio detection for gas chromatography. *J Sep Sci* 29(12):1946–1961.
16. Kahl BC (2010) Impact of Staphylococcus aureus on the pathogenesis of chronic cystic fibrosis lung disease. *Int J Med Microbiol* 300(8):514–519.
17. Goss CH, Muhlebach MS (2011) Review: *Staphylococcus aureus* and MRSA in cystic fibrosis. *J Cyst Fibros* 10(5):298–306.
18. Kushner DJ, Baker A, Dunstall TG (1999) Pharmacological uses and perspectives of heavy water and deuterated compounds. *Can J Physiol Pharmacol* 77(2):79–88.
19. Cowley ES, Kopf SH, LaRiviere A, Ziebis W, Newman DK (2015) Pediatric cystic fibrosis sputum can be chemically dynamic, anoxic, and extremely reduced due to hydrogen sulfide formation. *MBio* 6(4):e00767.
20. Palmer KL, Aye LM, Whiteley M (2007) Nutritional cues control *Pseudomonas aeruginosa* multicellular behavior in cystic fibrosis sputum. *J Bacteriol* 189(22):8079–8087.
21. Zhang X, Gillespie AL, Sessions AL (2009) Large D/H variations in bacterial lipids reflect central metabolic pathways. *Proc Natl Acad Sci USA* 106(31):12580–12586.
22. Dengremont E, Membré JM (1995) Statistical approach for comparison of the growth rates of five strains of *Staphylococcus aureus*. *Appl Environ Microbiol* 61(12):4389–4395.
23. Worlitzsch D, et al. (2002) Effects of reduced mucus oxygen concentration in airway *Pseudomonas* infections of cystic fibrosis patients. *J Clin Invest* 109(3):317–325.
24. Filkins LM, et al. (2015) Coculture of *Staphylococcus aureus* with *Pseudomonas aeruginosa* drives *S. aureus* towards fermentative metabolism and reduced viability in a cystic fibrosis model. *J Bacteriol* 197(14):2252–2264.
25. Gill CO, Suisted JR (1978) The effects of temperature and growth rate on the proportion of unsaturated fatty acids in bacterial lipids. *J Gen Microbiol* 104(1):31–36.
26. Cohen Z, Vonshak A, Richmond A (1988) Effect of environmental conditions on fatty acid composition of the red alga *Porphyridium cruentum*: Correlation to growth rate. *J Phycol* 24(3):328–332.
27. Kopf SH, et al. (2015) Heavy water and ^{15}N labelling with NanoSIMS analysis reveals growth rate-dependent metabolic heterogeneity in chemostats. *Environ Microbiol* 17(7):2542–2556.
28. Kempf VA, Trebesius K, Autenrieth IB (2000) Fluorescent in situ hybridization allows rapid identification of microorganisms in blood cultures. *J Clin Microbiol* 38(2):830–838.
29. Kiviet DJ, et al. (2014) Stochasticity of metabolism and growth at the single-cell level. *Nature* 514(7522):376–379.
30. Stewart MK, Cummings LA, Johnson ML, Berezow AB, Cookson BT (2011) Regulation of phenotypic heterogeneity permits *Salmonella* evasion of the host caspase-1 inflammatory response. *Proc Natl Acad Sci USA* 108(51):20742–20747.
31. Greenwood D (1985) Phenotypic resistance to antimicrobial agents. *J Antimicrob Chemother* 15(6):653–655.
32. Sanders DB, et al. (2010) Failure to recover to baseline pulmonary function after cystic fibrosis pulmonary exacerbation. *Am J Respir Crit Care Med* 182(5):627–632.
33. Zhang Y (2014) Persisters, persistent infections and the Yin-Yang model. *Emerging Microbes Infect* 3(1):e3.
34. Rao SPS, Alonso S, Rand L, Dick T, Pethe K (2008) The protonmotive force is required for maintaining ATP homeostasis and viability of hypoxic, nonreplicating Mycobacterium tuberculosis. *Proc Natl Acad Sci USA* 105(33):11945–11950.
35. Yano T, et al. (2011) Reduction of clofazimine by mycobacterial type 2 NADH:quinone oxidoreductase: A pathway for the generation of bactericidal levels of reactive oxygen species. *J Biol Chem* 286(12):10276–10287.
36. Harrison F (2007) Microbial ecology of the cystic fibrosis lung. *Microbiology* 153(Pt 4):917–923.
37. de Laeter JR, et al. (2003) Atomic weights of the elements. Review 2000 (IUPAC Technical Report). *Pure Appl Chem* 75(6):683–800.
38. Coplen TB (1988) Normalization of oxygen and hydrogen isotope data. *Chem Geol Isot Geosci Sect* 72(4):293–297.
39. Griffiths MJ, van Hille RP, Harrison STL (2010) Selection of direct transesterification as the preferred method for assay of fatty acid content of microalgae. *Lipids* 45(11):1053–1060.
40. Amann RI, Krumholz L, Stahl DA (1990) Fluorescent-oligonucleotide probing of whole cells for determinative, phylogenetic, and environmental studies in microbiology. *J Bacteriol* 172(2):762–770.
41. Hogardt M, et al. (2000) Specific and rapid detection by fluorescent in situ hybridization of bacteria in clinical samples obtained from cystic fibrosis patients. *J Clin Microbiol* 38(2):818–825.
42. Tajbakhsh S, et al. (2008) Detection of *Pseudomonas aeruginosa* in sputum samples by modified fluorescent in situ hybridization. *Afr J Biotechnol* 7(5):553–556.
43. Wallner G, Amann R, Beisker W (1993) Optimizing fluorescent in situ hybridization with rRNA-targeted oligonucleotide probes for flow cytometric identification of microorganisms. *Cytometry* 14(2):136–143.
44. Stoecker K, Dorninger C, Daims H, Wagner M (2010) Double labeling of oligonucleotide probes for fluorescence in situ hybridization (DOPE-FISH) improves signal intensity and increases rRNA accessibility. *Appl Environ Microbiol* 76(3):922–926.
45. Manz W, Amann R, Ludwig W, Wagner M, Schleifer KH (1992) Phylogenetic oligodeoxynucleotide probes for the major subclasses of proteobacteria: Problems and solutions. *Syst Appl Microbiol* 15(4):593–600.
46. Lathe R (1985) Synthetic oligonucleotide probes deduced from amino acid sequence data. Theoretical and practical considerations. *J Mol Biol* 183(1):1–12.
47. Florijn RJ, Slats J, Tanke HJ, Raap AK (1995) Analysis of antifading reagents for fluorescence microscopy. *Cytometry* 19(2):177–182.
48. Zhao J, et al. (2012) Impact of enhanced Staphylococcus DNA extraction on microbial community measures in cystic fibrosis sputum. *PLoS One* 7(3):e33127.
49. Caporaso JG, et al. (2011) Global patterns of 16S rRNA diversity at a depth of millions of sequences per sample. *Proc Natl Acad Sci USA* 108(Suppl 1):4516–4522.
50. Edgar RC (2010) Search and clustering orders of magnitude faster than BLAST. *Bioinformatics* 26(19):2460–2461.
51. Chen SS, Sperling E, Silverman JM, Davis JH, Williamson JR (2012) Measuring the dynamics of *E. coli* ribosome biogenesis using pulse-labeling and quantitative mass spectrometry. *Mol Biosyst* 8(12):3325–3334.
52. Kreiswirth BN, et al. (1983) The toxic shock syndrome exotoxin structural gene is not detectably transmitted by a prophage. *Nature* 305(5936):709–712.
53. Yuan Y, Leeds JA, Meredith TC (2012) *Pseudomonas aeruginosa* directly shunts β-oxidation degradation intermediates into de novo fatty acid biosynthesis. *J Bacteriol* 194(19):5185–5196.
54. Yuan Y, Sachdeva M, Leeds JA, Meredith TC (2012) Fatty acid biosynthesis in *Pseudomonas aeruginosa* is initiated by the FabY class of β-ketoacyl acyl carrier protein synthases. *J Bacteriol* 194(19):5171–5184.
55. Kaneda T (1991) Iso- and anteiso-fatty acids in bacteria: Biosynthesis, function, and taxonomic significance. *Microbiol Rev* 55(2):288–302.
56. Easteal AJ, Edge A, Woolf LA (1984) Isotope effects in water. Tracer diffusion coefficients for $H_2^{18}O$ in ordinary water. *J Phys Chem* 88(24):6060–6063.
57. Kreuzer-Martin HW, Lott MJ, Ehleringer JR, Hegg EL (2006) Metabolic processes account for the majority of the intracellular water in log-phase *Escherichia coli* cells as revealed by hydrogen isotopes. *Biochemistry* 45(45):13622–13630.
58. van Bodegom P (2007) Microbial maintenance: A critical review on its quantification. *Microb Ecol* 53(4):513–523.
59. Polerecky L, et al. (2012) Look@NanoSIMS—;A tool for the analysis of NanoSIMS data in environmental microbiology. *Environ Microbiol* 14(4):1009–1023.
60. Musat N, et al. (2014) The effect of FISH and CARD-FISH on the isotopic composition of ^{13}C- and ^{15}N-labeled Pseudomonas putida cells measured by nanoSIMS. *Syst Appl Microbiol* 37(4):267–276.
61. Wang Y, Sessions AL (2008) Memory effects in compound-specific D/H analysis by gas chromatography/pyrolysis/isotope-ratio mass spectrometry. *Anal Chem* 80(23):9162–9170.